# Enhanced humidity pockets originating in the mid boundary layer as a mechanism of cloud formation below the lifting condensation level



2017 Environ. Res. Lett. 12 024020

(http://iopscience.iop.org/1748-9326/12/2/024020)

Environmental Research Letters

LETTER

# Enhanced humidity pockets originating in the mid boundary layer as a mechanism of cloud formation below the lifting condensation level

Eitan Hirsch[1,2], Ilan Koren[1,4], Orit Altaratz[1], Zev Levin[3] and Eyal Agassi[2]

[1] Department of Earth and Planetary Sciences, Weizmann Institute, Rehovot 76100, Israel
[2] Department of Environmental Physics, Israel Institute for Biological Research, Nes-Ziona, Israel
[3] Department of Geosciences, Tel-Aviv University, Tel-Aviv, Israel
[4] Author to whom any correspondence should be addressed.

**E-mail:** ilan.koren@weizmann.ac.il

**Keywords:** small clouds, humidity perturbations, cloud formation mechanism

Supplementary material for this article is available online

OPEN ACCESS

RECEIVED
26 April 2016

REVISED
22 January 2017

ACCEPTED FOR PUBLICATION
24 January 2017

PUBLISHED
20 February 2017



## Abstract

A ground-based field campaign was conducted during the summer of 2011, 10 km east of the Israeli coast, aimed at studying small, warm convective clouds. During the campaign, clouds were detected on days that were predicted to be cloud-free by standard forecasting methods. Moreover, the clouds' bases were often much lower than the estimated lifting condensation level. Detailed air parcel model simulations revealed that such small non-buoyant clouds can form only if the convective motion is driven by perturbations in the relative humidity in the middle of the boundary layer, rather than by temperature perturbations near the surface. Furthermore, cloud base height exhibited weak sensitivity to the initial elevation of the parcel, suggesting that it serves as an accumulation point for many relative-humidity-perturbed thermodynamic trajectories. Such a mechanism is likely to be common under atmospheric conditions of a hot and humid boundary layer capped by a strong inversion layer.

## 1. Introduction

A ground-based field campaign was conducted 10 km east of the Mediterranean coast in central Israel during the summer of 2011 to measure small warm convective clouds and retrieve their spatial, optical and microphysical properties (Hirsch *et al* 2014, 2015). Convective clouds form when an air parcel rises in the atmosphere, expands, cools down and creates supersaturation conditions. The lifting condensation level (LCL, Bolton 1980) is a good predictor of convective clouds' base height (Craven *et al* 2002). A strong thermal inversion layer located below the LCL can block the upward motion of a rising parcel and prevent the cloud's formation. The atmospheric profile shown in figure 1(*a*) presents a typical midday summertime profile in Israel that was measured during the campaign (1 Jun 2011, 15:00 local time), where hot and humid air was capped by an inversion layer.

This date demonstrates a case in which no cloud formation was predicted by standard forecasting methods, due to the location of a low inversion layer below the estimated height of the LCL (green line), that is likely to suppress vertical parcels' motion. However, in this case, as well as in many others with similar conditions, clouds were indeed measured (figure 1(*b*)). Moreover, the measured cloud base height on those days was much lower than the calculated LCL (as will be shown further on in section 3). The measured clouds were characterized by small liquid water paths ($<50$ g m$^{-2}$), small effective radii (a few microns), and short lifetimes (a few minutes) (Hirsch *et al* 2014). Previous work (Hirsch *et al* 2015) showed that small warm clouds dominate the cloud radiative properties during the summer over the studied region. These clouds contributed 83% of the clouds' reflectance, and their average daily radiative effect was estimated to be $-3.6$ W m$^{-2}$.

Boundary layer cloud formation is tightly coupled to the structure of the subcloud layer. LeMone and Pennell (1976) showed that the distribution of trade cumulus clouds is determined by the structure of the

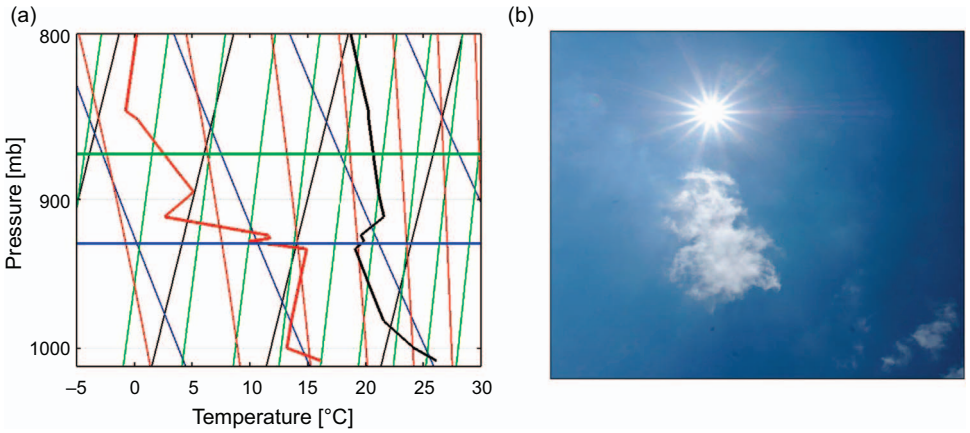


**Figure 1.** (*a*) The temperature (black) and dew point (red) profiles on 1 Jun 2011 at 15:00 local time, measured at the Bet-Dagan meteorological station. Note that the LCL (horizontal green line) is located far above a strong thermal inversion layer. Such conditions suggest no cloud formation. Nevertheless, clouds were measured during that time. (*b*) Image of a small cloud taken on the same date at 15:12 local time. The size of the cloud is ∽100 m. Clouds were also documented by ceilometer readings. The horizontal blue line in (a) is the measured cloud base height. Note the clear discrepancy between the predicted cloud base height (at the LCL) and the measured one.

subcloud layer and its moisture fluxes. They noted that suppressed small clouds are the result of moist buoyant air parcels which are collected by the updraft of organized circulations in the subcloud layer. Siebesma and Cuijpers (1995) used Large Eddy Simulations (LES) results to demonstrate that the positive vertical velocity in boundary-layer clouds is due to acceleration in the well-mixed subcloud layer. Other studies (Nicholls and Lemone 1980, Seifert and Heus 2013) have shown that convective elements in the marine subcloud layer are usually colder but wetter than their surrounding air. Several cloud field model studies have treated the variability in temperature and humidity below the clouds in a statistical manner (Sommeria and Deardorff 1977, Mellor 1977, Neggers *et al* 2009a, 2009b). Those studies pointed out the importance of representing the subgrid-scale variability in humidity to obtain realistic results.

Other studies have focused on the shallow convective cloud layer. Using observations of trade cumulus cloud fields, Malkus (1958) showed that most of the clouds are colder, denser and more humid than their environment. She claimed that a small fraction of the cloudy area is actively buoyant (has positive buoyancy above the cloud base) and warmer than the environment. Bechtold and Cuijpers (1995) used LES to show that marine cumulus clouds are slightly colder than the environmental air. de Roode and Bretherton (2003) used LES results to demonstrate that clouds' mean temperature is usually lower than the mean environmental temperature, while the equivalent potential temperature may be higher. Heus and Jonker (2008) showed similar results, using both LES and aircraft measurements.

The mixed layer is commonly described as composed of thermals or plumes (Turner 1969, Stull 1988) that start the convective motion near the surface and create clouds while ascending above the LCL. As described above, a major proportion of boundary-layer clouds can be regarded as non-buoyant, passive or forced clouds (i.e. parcels with total negative buoyancy after ascending above the cloud base height, Stull 1988). Therefore, the formation of small non-buoyant clouds above the LCL can result from the overshoot of a thermal over the LCL that creates a pocket of supersaturation conditions. However, in this work we describe clouds that are located below the LCL, and we propose a different mechanism for their formation under thermodynamic conditions that predict a cloud-free sky.

## 2. Methods

Aiming to resolve the evolution of small buoyant air parcels that ascend due to weak perturbations in temperature or humidity, a unique detailed parcel model was developed to resolve the growth of haze particles (with a given size distribution) into cloud droplets (see detailed description in Hirsch *et al* 2014). The model employs fundamental thermodynamic and microphysical equations. It iteratively solves the equations for the energy budget of the parcel, the growth of the haze particles (and later of the cloud droplets), and the updraft and relative humidity (RH) of the parcel. The growth rate of the haze and cloud droplets is determined by the diffusion equation for every droplet in the rising parcel, and the first law of thermodynamics is solved explicitly to account for latent heat release by the condensation on both the haze and cloud droplets. As presented in Hirsch *et al* (2014), the model successfully predicted the existence of a unique type of convective cloud (referred as 'transition zone cloud') which is composed of a mixture of haze and cloud droplets.

The model was initialized with atmospheric sounding measurements obtained by the Israeli Meteorological Service at the Bet-Dagan meteorological station, which is located 10 km east of the Mediterranean shore. The atmospheric profiles used

in the analysis were measured at 12:00 UTC (15:00 local time). The LCL was derived by two different methods: 1) using the average value of the lowest 500 m of the atmosphere (hereafter, average LCL). This method is used by the University of Wyoming (http://weather.uwyo.edu/upperair/sounding.html), and 2) using the surface properties as described by Bolton (1980) and Stull (1988):

$$T_{\mathrm{LCL}} = \frac{1}{\frac{1}{T_K - 55} - \frac{\ln\left(\frac{\mathrm{RH}}{100}\right)}{2840}} + 55$$

$$P_{\mathrm{LCL}} = P\left(\frac{T_{\mathrm{LCL}}}{T_K}\right)^{3.5}$$

where $T_k$, $P$ and RH are the temperature, pressure and relative humidity, respectively, of the air parcel at ground level (hereafter, ground LCL).

Cloud base measurements, taken by a ceilometer (Vaisala Model CL31) located at the Bet-Dagan station, were used as well. A 2 h average of the 10 min readings was used to determine the measured cloud base height around the time of the atmospheric profile measurement.

## 3. Results

We simulated two different mechanisms for convection initiation. In the first scheme, the air parcel was subjected to a perturbation in temperature (compared to the ambient conditions), simulating convective cloud initiation by thermals (as widely simulated in convective cloud models). However, an increase in parcel temperature is not the only mechanism by which positive buoyancy can be gained. An increase in the RH of the parcel decreases its density, also resulting in increased buoyancy. Therefore, in the second initialization scheme, the parcel was subjected to a perturbation in RH (relative to ambient conditions). No initial updraft was applied to the parcels in either scheme.

The simulations' algorithm is presented here as follows: for a given profile (of temperature $T$, and dew point $T_d$), parcel lifting is initiated by a perturbation in either temperature or humidity. The perturbation is gradually increased until the parcel is lifted up to a saturation level (marking the predicted cloud base height). The parcel movement starts at a range of heights within the boundary level (50 m to 700 m in increments of 50 m). For each initial height, once the perturbation is large enough to lift the parcel to a condensation level, the parcel's initial height, perturbation and the predicted cloud base height are stored and we move to the next (higher) initial height. The results are plotted in figure 2 together with the temperature (blue) and RH (red) profiles, the theoretical LCL range (cyan horizontal line represents the ground base LCL estimation as described in equation (1) and the magenta horizontal line represents the lowest 500 m average LCL, as used in the University of Wyoming database), and the ceilometer-measured cloud base height (blue horizontal line) during the radiosonde release time. The initial and predicted cloud base heights of each simulation are plotted as pairs of points with the same color, and mark the initial perturbation by distance from the relevant profile. For example, considering temperature perturbation for the case of 6 Aug 2011 (figure 2(*c*)): if a perturbation of $\Delta T$ = 1.25 °C is sufficient to lift a parcel from an initial height of 50 m, with environmental temperature of $T$(50 m) = 31.25 °C, to create a cloud base height at 1338 m, then a same-colored pair of points (blue circles, figure 2(*c*)) is drawn, one at 50 m and one at 1338 m with a temperature of $T + \Delta T$ = 32.5 °C. Or if we consider RH perturbations for the 11 Jun 2011 case (figure 2(*b*)): if $\Delta$RH = 0.4% is sufficient to lift a parcel from an initial height of 50 m, with environmental RH of RH(50 m) = 54.6%, to create a cloud base height at 1294 m, then a same-colored pair of points (blue circles, figure 2(*b*)) is drawn, one at 50 m and one at 1294 m with a RH of RH + $\Delta$RH = 55%.

An increase in the parcel's temperature leads to a decrease in its RH, which dictates higher lifting before the parcel reaches saturation. It is therefore notable that in all of the thermal perturbation tests, for both case studies examined here (figures 2(*a*) and (*c*)), the simulated cloud base was significantly higher than the cloud base simulated by RH perturbations and the measured height (blue horizontal line), regardless of the initial height of the parcel and the magnitude of the thermal perturbation.

The simulations that were initiated by raising the parcel's RH compared to the environment (RH perturbations, figures 2(*b*) and (*d*)) yielded different results. Parcels that started near the surface (in the lower 150 m of the atmosphere) did not form clouds at altitudes that approximated the measured heights (697 m for 6 Aug 2011 and 884 m for 11 Jun 2011). However, all of the parcels that ascended from an initial height of 200–600 m above the surface and were subjected to RH perturbation in the range of 5.5%–8.2% created clouds near the measured height.

Our results revealed that for a wide range of initial heights within the boundary layer, the simulated cloud base height converges to a narrow range around the measured height. The fact that under the minimal RH perturbation required to reach saturation level, the measured cloud base height served as an accumulation point for the predicted cloud base heights of the simulated parcels sheds light on a basic property of such clouds. To explain this, we explored parcel trajectories in two phase spaces: i) vertical velocity versus differences in the virtual temperature ($\Delta T_v$) and ii) clouds base height versus $\Delta T_v$. $\Delta T_v$ is a measure of the parcel's buoyancy, taking into account

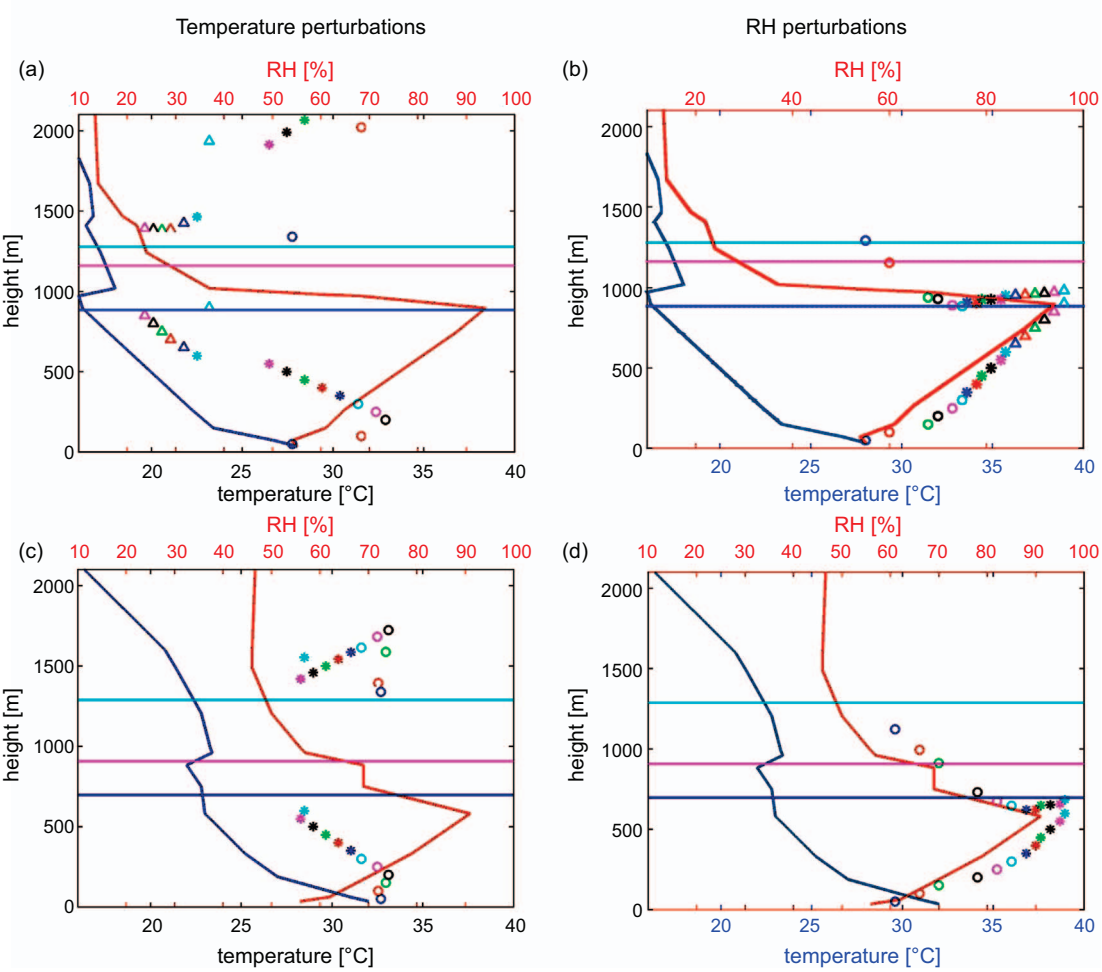


**Figure 2.** The results of a detailed parcel model for two case studies: 11 Jun 2011 (*a*), (*b*) and 6 Aug 2011 (*c*), (*d*) both cases for 15:00 local time. (*a*), (*c*) Temperature perturbations and (*b*), (*d*) RH perturbations. In every graph, the cyan and magenta horizontal lines represent the ground and average LCL, respectively, and the horizontal blue line represents the measured cloud base height. The initial parcel height and the magnitude of the perturbation are represented by the location on the graph compared to the environmental profile. The paired symbols represent the air parcel model results for various initial heights and perturbations and the cloud base heights of the resulting clouds (see explanation in text).

differences in both temperature and RH between the parcel and its environment; it therefore determines the parcel's acceleration. Figure 3 shows the trajectories for the parcels presented in figure 2. All trajectories start from the zero updraft point (lowest point on the right) and end when the parcels reach 100% RH (minimal $\Delta T_v$ values on the left). Analyzing the temperature perturbations first (figures 3(*a*) and (*c*)), we note that a relatively large initial $\Delta T_v$ is needed for cloud formation (shown also as the distance between the cloud base point and the temperature profile in figure 2). As already noted, an increase in the parcel's temperature reduces its RH and therefore dictates a longer path to reach saturation. The large initial $\Delta T$ results in a relatively large increase in the parcel's buoyancy; this drives stronger updrafts, allowing the parcels to penetrate the inversion layer and reach saturation at different heights (which are all higher than the LCL and measured cloud base height in any case). Labels 1–4 in figure 3(*a*) indicate different stages during the vertical ascent of a specific parcel, as follows. (1) The parcel starts to ascend. Since the atmospheric thermal lapse rate at those heights is very close to the dry adiabatic one, the parcel accelerates while $\Delta T_v$ remains relatively constant. (2) When the parcel reaches the thermal inversion layer, it quickly loses its buoyancy ($\Delta T_v$ decreases), and (3) starts to decelerate. (4) The parcel continues to move upward until it reaches saturation and becomes a cloud. It is interesting to note that, at the level at which the parcels become clouds, their $\Delta T_v$ is negative, and the updraft is very small (soon to become downdraft). On the other hand, an increase in RH can be viewed as a delicate reduction of the parcel's density with no effect on the thermal terms (to a good approximation). Parcels that were initiated by RH perturbations (figures 3(*b*) and (*d*)) require much smaller initial $\Delta T_v$ to form clouds. Therefore, the derived updrafts are weaker, and the parcels ascend much more slowly (note the small updraft and the small updraft variance) and are more easily blocked within the inversion layer. Similar buoyancy values imply that the parcels reach the inversion with a similar momentum and therefore will decelerate and stop at a similar level within the

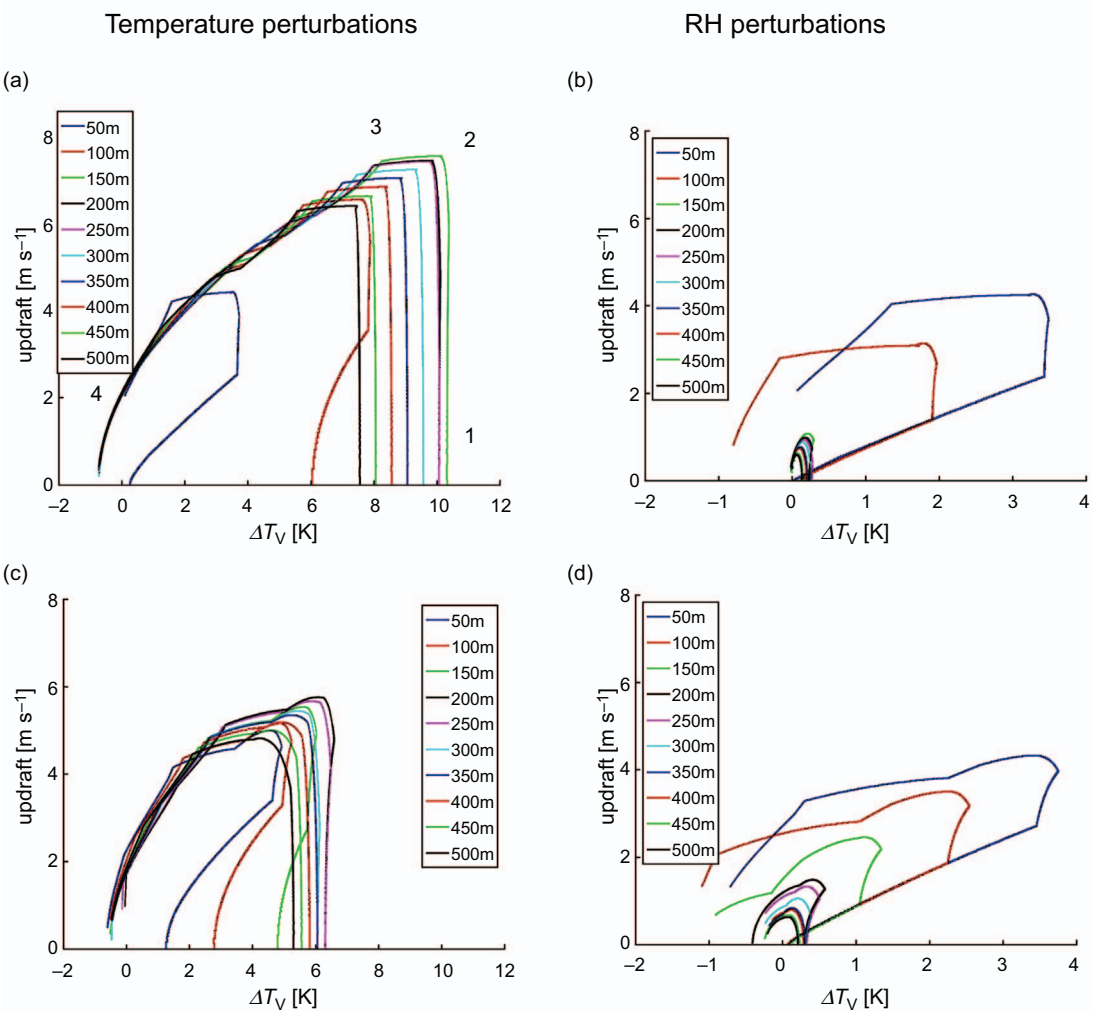


**Figure 3.** Detailed temporal analysis of the parcels' motion for temperature (*a*), (*c*) and RH (*b*), (*d*) perturbations on 11 Jun 2011 (*a*), (*b*), and 6 Aug 2011 (*c*), (*d*). The *y*-axis is the updraft of the parcel, and the *x*-axis is the difference in virtual temperature between the parcel and the environment ($\Delta T_v$). Every curve in the graphs represents a parcel that was initiated at a different height. At every height, the parcel with the minimal perturbation that led to the formation of a cloud is presented. The labels 1–4 in panel a represent different stages during the vertical ascent of a specific parcel: 1—initiation of the vertical motion, 2—parcel reaches the thermal inversion layer, 3—parcel starts to decelerate, 4—parcel reaches saturation and becomes a cloud.

inversion. Nevertheless, the additional RH (∽5%–8%) that initiated the parcel's ascent is sufficient to form a cloud, as the parcels decelerate to an almost complete stop at similar heights. Similar analysis of the parcels' trajectories in the phase space of cloud base height versus $\Delta T_v$ (figure S1 (stacks.iop.org/ERL/12/024020/mmedia) in the supporting information (SI)) provides a complementary view of the problem. It shows that the large $\Delta T_v$ required for cloud formation of the temperature-perturbed parcels dictates a higher cloud base height, whereas parcels that are lifted by RH perturbations in the middle of the boundary layer ascend with a small and similar $\Delta T_v$ range, implying weak updrafts with small variance. As a result, while they approach saturation, the inversion layer blocks them at similar heights.

How common is this type of warm, small cloud? figure 4 presents the LCL and measured cloud base height (blue) during the summer months in Bet Dagan (1 Jun–31 Aug 2011). On 27 out of 92 d, clouds were measured between 11:00 UTC and 13:00 UTC (14:00–16:00 local time) in a significantly lower position than the estimated LCL (with an average difference of 363 m). This finding suggests that the conditions considered in our simulations are quite common, as is the existence of clouds below the ambient LCL. Our model was further used to calculate the expected cloud base height for every atmospheric profile on these 27 d of the field campaign. Using the RH perturbation scheme and initiating the parcels at 400 m yielded calculated cloud base heights (green circles in figure 4) that were very similar to the measured ones (blue circles in figure 4). The initial height of 400 m was chosen as a mid-level height in the boundary layer for that season. The average absolute difference between the calculated and measured cloud base height was ∽70 m.

## 4. Discussion and summary

This paper studies the formation of a special subset of small, warm convective clouds that are often too small

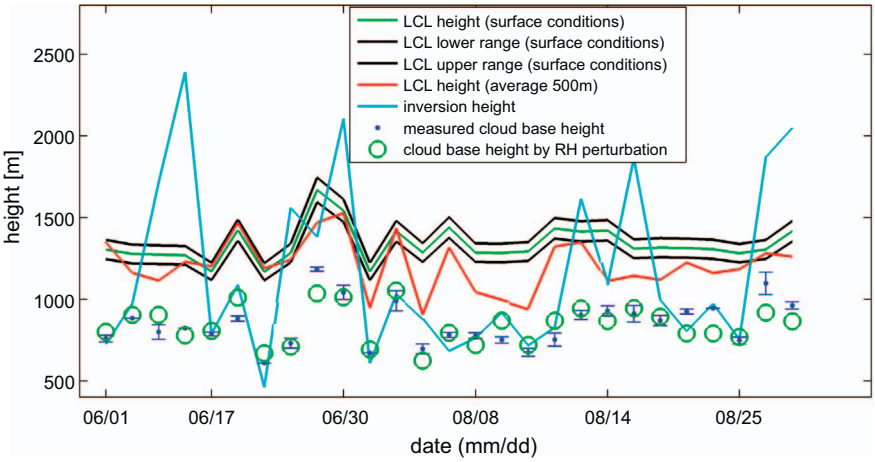


**Figure 4.** Seasonal (June–August 2011) analysis of the LCL range (green, black and red lines) and the measured cloud base height (blue circles). The upper and lower LCL range (black lines) were calculated by introducing perturbations of ±5 °C and ±10% of the surface measured temperature and RH (respectively), and taking the maximal and minimal LCL retrieved by these perturbations. The error bars on the cloud base height points represent the measured standard deviation in the cloud base height during a 2 h period (14:00–16:00 local time). The inversion layer base height is presented as well (cyan). Note that during most of the campaign, the LCL was higher than the base of the inversion layer. The calculated cloud base height by initiating a parcel at 400 m with RH perturbation is marked by green circles. The average difference between the standard LCL calculations and the measured cloud base height was 363 m, whereas the average difference between the measured and the model-simulated RH perturbed cloud base height is 70 m.

to be detected (Koren *et al* 2008). Sparse cloud fields composed of small clouds are often below the spatial resolution of standard cloud detectors and therefore might be classified as cloud-free regions. We show that these clouds can form under atmospheric conditions in which the predicted LCL is significantly higher than the base of the inversion layer. Such clouds were measured on 27 out of 92 d during summer 2011 field measurements, 10 km east of the Mediterranean coast in central Israel. We show that the origin of the convective motion is likely to be humidified pockets located aloft in the mixing layer, rather than thermals ascending from near the surface. Processes that drive variability in specific (and therefore in relative) humidity are in the focus of many studies that tried to better represent clouds in GCM models (Lin 2014). The turbulent nature of the boundary layer and convection are the main processes that drive the variance in the humidity (Couvreux *et al* 2005). Studies dedicated to measure the variance in specific humidity under variety of atmospheric conditions have shown relatively large perturbations with characteristic time scale of minutes (Price 2001). Aircrafts (Ek and Mahrt 1994), surface (Sempreviva and Gryning 1996) and 3D scanning differential absorption lidar (Späth *et al* 2016) studies reported on RH fluctuations of more than 10% in the boundary layer, which support the possible initiation of such humidified pockets.

In order to minimize possible sources of errors in our measurements, cloud base height was retrieved by a ceilometer (Vaisala, CL31), with a vertical resolution of 5 m. The parcel model was initialized with atmospheric profiles that were measured by standard radiosondes (by the Israeli Meteorological Service). The measured atmospheric profiles are confined spatially and cannot account for the natural variance within the field. To estimate possible variance effects, we introduced perturbations of ±5 °C and ±10% to the surface measured temperature and RH (respectively) and calculated the LCL response (marked in black lines as the upper and lower LCL range in figure 4). It is notable that such variance is the LCL estimations cannot provide explanation for the measured clouds base heights.

Detailed case studies are presented of small convective cloud formation on days when the measured cloud base was far below the calculated LCL. A new parcel model, tuned to resolve the details of haze particle growth into cloud droplets, was used to describe the formation of such non-buoyant clouds. The model calculates, using first principles, the parcel's updraft, temperature and relative humidity, such that for parcels that do reach saturation, the exact location of the cloud base is fully resolved. Our results show that only parcels originating around the middle of the boundary layer whose vertical motion is initiated by RH perturbations can form small clouds much below the LCL around the observed cloud base levels. Moreover, it was shown that the delicate RH perturbations initiate weak buoyancy that is insensitive to parcel initiation height. Therefore, parcels originating at a range of heights in the middle of the boundary layer will all form clouds around the same level, in good agreement with the observations. We noted that the small variances in the measured cloud base height, all below the LCL (indicated by the blue error bars in figure 4), further reinforce the hypothesis that these clouds are the result of RH perturbations in the middle of the boundary layer. We showed that when thermal perturbation is the driving mechanism, the calculated cloud bases are significantly higher than

the theoretical LCL, with larger variability; they are therefore much higher than the observed cloud bases. The effect of entrainment of dry air from the parcel's surrounding, into the moist air within the parcel, is estimated with a sink term in the updraft derivative (Hirsch *et al* 2014). The entrainment sink term is proportional to the 2nd power of the parcel's velocity (Lee and Pruppacher 1977). To better understand the results' sensitivity to RH dilution by entrainment, as shown in the SI (figure S2), we have implemented additional dilution term that is proportional to the RH differences between the parcel and its surroundings. The dilution reduces the updrafts and therefore some of the parcels may not have enough momentum to reach the level of saturation. But for parcels that do reach saturation the effect on the saturation level (cloud base level) is relatively small (∽10 m).

The specific atmospheric conditions discussed here are quite common during the summer in the eastern Mediterranean region. Moreover, a hot and humid boundary layer that is capped by a strong inversion layer is not unique. Many coastal areas along the subtropical belts are characterized by such conditions (Dima and Wallace 2003). Profiles of two examples of such conditions, from Palma de Mallorca and Tenerife, are shown in the SI (figure S3). Similar to what is seen over Israel, ceilometer data in those two examples showed that the measured cloud base height is located a few hundred meters below the LCL, suggesting that the formation mechanism presented here may be quite general.

## Acknowledgments

The research leading to these results received funding from the European Research Council (ERC) under the European Union's Seventh Framework Programme (FP7/2007–2013)/ERC Grant agreement no. 306965 (CAPRI).

We thank the University of Wyoming, Department of Atmospheric Sciences for the sounding data (downloaded from http://weather.uwyo.edu/upperair/sounding.html).

We also thank the Israeli Meteorological Service for providing us with the ceilometer and radiosonde data.

## References

Bechtold P and Cuijpers J W 1995 Cloud perturbations of temperature and humidity: a LES study *Boundary Layer Meteorol.* **76** 377–86

Bolton D 1980 The computation of equivalent potential temperature *Mon. Weather Rev.* **108** 1046–53

Craven J P, Jewell R E and Brooks H E 2002 Comparison between observed convective cloud-base heights and lifting condensation level for two different lifted parcels *Weather Forecast.* **17** 885–90

Couvreux F, Guichard F, Redelsperger J-L, Kiemle C, Masson V, Lafore J-P and Flamant C 2005 Water-vapour variability within a convective boundary-layer assessed by large-eddy simulations and IHOP_2002 observations *Q. J. R. Meteorol. Soc.* **131** 2665–93

de Roode S R and Bretherton C S 2003 Mass-flux budgets of Shallow Cumulus clouds *J. Atmos. Sci.* **60** 137–51

Dima Ioana M and Wallace J M 2003 On the seasonality of the Hadley cell *J. Atmos. Sci.* **60** 1522–7

Ek M and Mahrt L 1994 Daytime evolution of relative-humidity at the boundary-layer top *Mon. Weather Rev.* **122** 2709–21

Heus T and Jonker H J J 2008 Subsiding Shells around Shallow cumulus clouds *J. Atmos. Sci.* **65** 1003–18

Hirsch E, Koren I, Levin Z, Altaratz O and Agassi E 2014 On transition-zone water clouds *Atmos. Chem. Phys.* **14** 9001–12

Hirsch E, Koren I, Altaratz O and Agassi E 2015 On the properties and radiative effects of small convective clouds during the eastern Mediterranean summer *Environ. Res. Lett.* **10** 044006

Koren I, Oreopoulos L, Feingold G, Remer L A and Altaratz O 2008 How small is a small cloud? *Atmos. Chem. Phys.* **8** 3855–64

Lee I-Y and Pruppacher H 1977 A comparative study on the growth of cloud drops by condensation using an air parcel model with and without entrainment *Pure Appl. Geophys.* **115** 523–45

LeMone M A and Pennell W T 1976 The relationship of trade wind cumulus distribution to sub-cloud layer fluxes and structure *Mon. Wea. Rev.* **104** 524539

Lin Y 2014 Humidity variability revealed by a sounding array and its implications for cloud representation in GCMs *J. Geophys. Res. Atmos.* **119** 499–10 514

Malkus J S 1958 On the structure of the trade-wind moist layer *Papers on Physical Oceanography and Meteorology* vol **13** (Woods Hole, MA: Massachusetts Institute of Technology and Woods Hole Oceanographic Institute) p 47

Mellor G L 1977 The Gaussian cloud model relations *J. Atmos. Sci.* **34** 356–8

Neggers Roel A J, Köhler M and Beljaars Anton C M 2009a A dual mass flux framework for boundary layer convection. Part I: transport *J. Atmos. Sci.* **66** 1465–87

Neggers Roel A J 2009b A dual mass flux framework for boundary layer convection. Part II: clouds *J. Atmos. Sci.* **66** 1489–506

Nicholls S and Lemone M A 1980 The fair weather boundary layer in GATE: the relationship of subcloud fluxes and structure to the distribution and enhancement of cumulus clouds *J. Atmos. Sci.* **37** 2051–67

Price J D 2001 A study of probability distributions of boundary-layer humidity and associated errors in parametrized cloud-fraction *Q.J.R. Meteorol. Soc.* **127** 739–58

Seifert A and Heus T 2013 Large-eddy simulation of organized precipitating trade wind cumulus clouds *Atmos. Chem. Phys* **13** 5631–45

Sempreviva A M and Gryning S-E 1996 Humidity fluctuations in the marine boundary layer measured at a coastal site with an infrared humidity sensor *Bound. Lay. Meteorol.* **77** 331–52

Siebesma A and Cuijpers J 1995 Evaluation of parametric assumptions for shallow cumulus convection *J. Atmos. Sci.* **52** 650–66

Sommeria G and Deardorff J W 1977 Subgrid-scale condensation in models of nonprecipitating clouds *J. Atmos. Sci.* **34** 344–55

Späth F, Behrendt A, Muppa S K, Metzendorf S, Riede A and Wulfmeyer V 2016 3-D water vapor field in the atmospheric boundary layer observed with scanning differential absorption lidar *Atmos. Meas. Tech.* **9** 1701–20

Stull R B 1988 *An Introduction to Boundary Layer Meteorology* (Dordrecht: Kluwer) p 666

Turner J S 1969 Buoyant plumes and thermals *Annu. Rev. Fluid Mech.* **1** 29–44